Experimental Design of a UCAV-based High Energy Laser Weapon

Antonios Lionis[a], Keith Cohn[b], and Conor Pogue[c]

[a]*Lieutenant HN, Electronics Department Head, HS Nikiforos Fvkas, Salamina Naval Base, Greece*
[b]*Senior Lecturer, Department of Physics, Naval Postgraduate School, Monterey CA, USA*
[c]*Research Assistant, Directed Energy Group, Department of Physics, Naval Postgraduate School, Monterey CA, USA*

Abstract. This study simulates a notional Unmanned Combat Aerial Vehicle (UCAV) based High Energy Laser (HEL) weapon using the laser beam atmospheric propagation simulation tool *WaveTrain* in a specified mission scenario for different laser configurations and engagement tactics. Design of Experiments (DOE) are applied to identify the statistically significant parameters of the laser weapon performance and to study the interaction between multiple parameters. Irradiance and power-in-the-bucket (PIB) on the target are used as the measures of performance (MOPs). Based on the statistical analysis, we identify two alternative HEL designs that under certain conditions could achieve equivalent performance and we estimate their corresponding weights. We then discuss the effect that HEL weight has on the endurance of the UCAV. Finally, additional simulation analysis examines the beam quality and jitter effects on the HEL performance.

INTRODUCTION

The deployment of an HEL weapon has been attempted multiple times over the past five decades. Despite having faced major difficulties throughout these efforts, including the cancellation of many programs, their potential advantages are too promising to be ignored. A variety of platforms have been considered already for an HEL weapon to be integrated, each one for different missions and with different capabilities. Several programs in the past attempted to integrate an HEL weapon onto large aircraft but were ultimately cancelled. Recently, the interest has shifted from large aircraft to small tactical platforms, such as jet fighters and attack helicopters. Another special airborne platform that could potentially host and employ an HEL weapon is an Unmanned Combat Aerial Vehicle (UCAV). General Atomics Aeronautical Systems, Inc., is currently working on this project, and company executives claim that it could be a reality in 2017 (Defense One 2015).

The combination of these two systems could potentially result in a game changing weapon. An HEL weapon shoots "bullets" that travel at speed of light, provides a deep magazine (almost unlimited ammunition), has a very low cost per shot, and has high accuracy (that mitigates the risk of collateral damages) (O' Rourke 2015). Furthermore, since UAVs have increased survivability with zero risk of human losses, and increased endurance and lower operational cost compared to manned aircrafts, they are attractive candidates to consider as an HEL platform.

The motivation of this study is to simulate a UCAV armed with an HEL weapon and develop a model for the engineering design of the system. Several design parameters of both the UCAV and the HEL may drastically affect the system's performance. The large number of simulation runs required to sufficiently explore all these design parameters and the considerable computation time of each simulation run do not allow a one-factor-at-a-time (OFAT) approach. Instead, a much more efficient way to gather the maximum information from a limited number of runs is applied; specifically, a type of Design of Experiments (DOE) called the Response Surface Methodology (RSM). This approach allows for determination of the significance of each design parameter and any potential correlations.

A laser beam atmospheric propagation simulation software tool called WaveTrain is utilized to simulate the UCAV-based HEL weapon in a specified mission scenario; the figures of merit extracted from the WaveTrain results are peak irradiance and PIB at the target. WaveTrain is a code suite that provides computer modeling of optical propagation though the turbulent atmosphere and is developed by MZA (Coy 2013). The simulation results are analyzed using the statistical software tool Minitab, which allows for the input and manipulation of statistical data, as well as the identification of trends and patterns in the results. The damage criteria will be estimated to give an idea of the required irradiance and power-in-the-bucket (PIB) the weapon has to achieve on the target's surface to melt a 5cm radius hole in a 3mm thick aluminum sheet. We also use a Matlab-based code called ANCHOR, developed by the Naval Postgraduate School's Directed Energy Group, to examine the effects of beam quality and platform jitter.

The design parameters we explore in this paper are the HEL output power and beam director's aperture size, as well as the UCAV's altitude, speed, and direction. We also explore the effects of the laser's beam quality and platform's jitter in a separate but related study. All but beam quality and jitter are explored using the DOE approach, while the last two are explored using ANCHOR.

ATMOSPHERIC PROPAGATION AND LETHALITY

In order to be able to estimate an HEL weapon's performance, one should thoroughly calculate the degradation of the beam travelling through the atmosphere to the target and the damage that the delivered energy will cause to the target. The three major atmospheric effects that cause the laser beam to degrade as it travels towards the target are atmospheric extinction (absorption and scattering), turbulence, and thermal blooming.

Atmospheric Extinction

Atmospheric extinction is the decrease of power in the beam due to the scattering and absorption effects in the atmosphere. The extinction coefficient is comprised of four parts: molecular absorption, molecular scattering, aerosol absorption, and aerosol scatter. The magnitude of the extinction coefficient depends heavily upon the wavelength of the laser beam, especially with respect to molecular absorption.

Figure 1, shows the extinction coefficient dependency on the wavelength, where we can identify a few transparency "windows" which would result in better propagation and therefore more lethal effects to target.
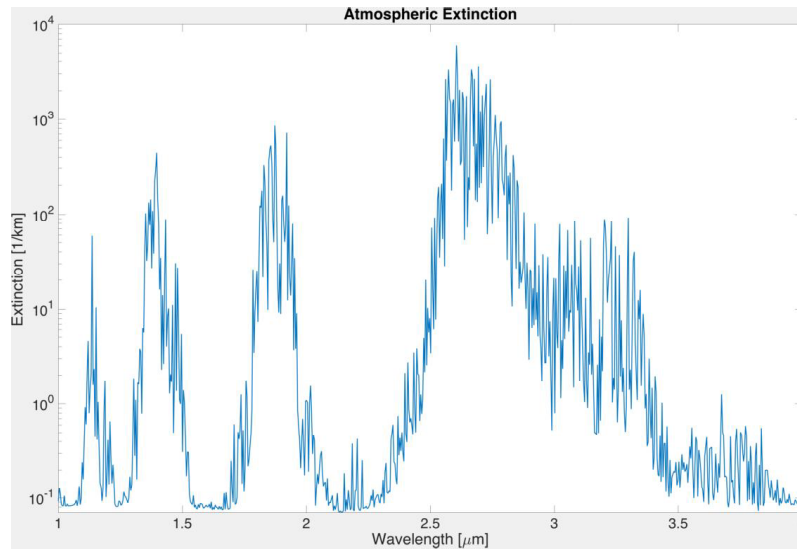
FIGURE 1. Atmospheric extinction coefficient as a function of wavelength. Large extinction coefficients result in strong attenuation of the beam. A transparency window is apparent for the typical solid-state lasers wavelength of 1.064nm. Source: Valiani (2016).

Atmospheric Turbulence

A laser beam propagating through the atmosphere is affected by turbulence that results in temperature and density variations. The temperature and density differences alter the air refractive index, and consequently the propagating beam is distorted due to induced amplitude and phase fluctuations. Turbulence, in general, has higher values near ground level. Therefore, platforms near the ground often experience strong turbulence right at the source, which then affects focusing downrange. On the other hand, operating a HEL weapon from a higher altitude, above much of the turbulence, could be advantageous.

Thermal Blooming

As the laser beam travels through the atmosphere, the atmospheric absorption will heat up the surrounding area, causing a change of the refractive index, which could cause the beam to defocus. This effect, which is higher as the output power of the weapon increases, is called thermal blooming. Obviously, for incoming targets from a constant bearing, thermal blooming may be a significant limiting factor.

Laser Lethality

The capability of a high energy laser weapon to cause any kind of damage or performance degradation through the delivery of its laser energy is called lethality. Apart from the energy delivered, the material of the target and its resistance to damage affects the lethality of the HEL weapon.

In order to estimate the effect of the laser, we have to account for the required heat energy needed to reach the melting temperature of the target,

$$Q_1 = c_P m \Delta T ,$$

(5)

where c_P the specific heat capacity of the target material, m the mass of the region on the target we wish to melt, and ΔT the temperature change needed to reach the melting point. Once the illuminated spot on the target has reached its melting temperature, we have to account for the energy needed to melt the specific material at the melting point,

$$Q_2 = m\Delta H \text{ ,}$$ (6)

where ΔH the heat of fusion of the target material. Thus, the total energy required to melt the target has to exceed the sum of Q_1 and Q_2. We can also take into consideration the loss mechanisms that remove power from the target area. One such mechanism is the power radiated away as a blackbody,

$$P_{rad} \approx \varepsilon\sigma A_r(T_{melt}^4 - T_{environment}^4),$$ (7)

 where ε the emissivity, σ the Stefan-Boltzmann constant, A_r the area being illuminated, T_{melt} the melting temperature of the target material, and $T_{environment}$ the ambient temperature of the air. The other mechanism is the power that is conducted to the surrounding volume of the target,

$$P_{cond} \approx kA_c(T_{melt} - T_{environment})/\Delta x,$$ (8)

where k the thermal conductivity, Δx the distance of temperature gradient, and A_c the area through which heat is being conducted away. As an illustrative example, we can compute the energy needed to melt a 3mm thick sheet of aluminum in a target area of radius 5cm. We assume the temperature gradient to be 2cm, a typical value for metals and dwell times of a few seconds. The basic properties of are shown in Table 1.

TABLE 1. Stainless Steel and Aluminum basic properties.

Parameter	Aluminum	Units
Density	$2.7*10^3$	kg/m3
Specific Heat Capacity	897	J/(kg*K)
Melting Temperature	933	K
Heat of Fusion	400	KJ/Kg
Emissivity	0.05	-
Stefan-Boltzmann constant	$5.67*10^{-8}$	$J/(m^2*s*K^4)$
Thermal Conductivity	237	W/(m*K)

Once we have calculated the required energy to melt the target and the total power losses, we can then estimate the required irradiance as follows:

$$I = \frac{\dfrac{Q_{melt} + Q_{heat}}{\tau_D} + P_{loss}}{A_r * \alpha_{abs}},$$ (9)

where $P_{loss} = P_{rad} + P_{cond}$, and τ_D is the dwell time (the time the laser illuminates the target area). Figures 2 and 3 show the accumulated irradiance and PIB for different dwell times. An additional

fractional absorption, α_{abs}, of 20% has been included to account for the fact that ~80% of the light may be reflected off the target.
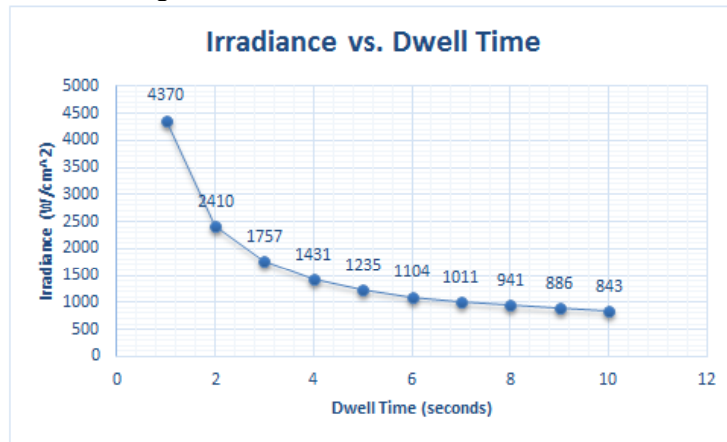
FIGURE 2. Estimated peak irradiance for a 3-mm thick aluminum sheet for various dwell times. Based upon the maximum laser dwell time, we can estimate the minimum value of peak irradiance required to melt the target.
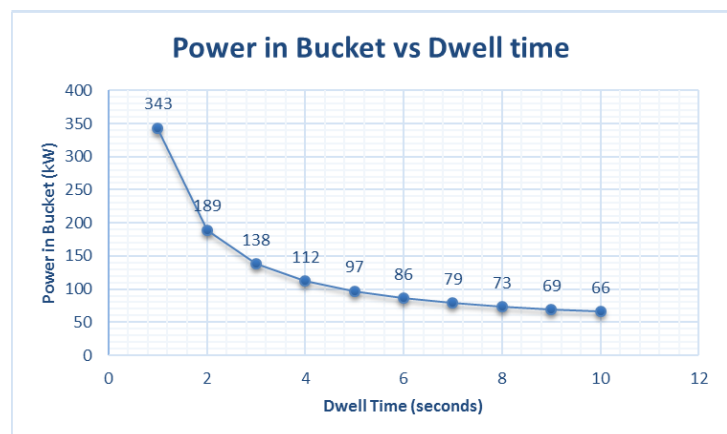
FIGURE 3. Power-in-the-bucket for a 3-mm thick aluminum sheet for various dwell times. Based upon the maximum laser dwell time, we can estimate the minimum value of PIB required to melt the target.

To achieve a dwell time of $\tau_D < 6$ seconds, we estimate the minimum peak irradiance to be approximately 1100W/cm^2 and the minimum PIB to be approximately 85kW.

EXPERIMENTAL DESIGN AND SIMULATION

Design of Experiments (DOE) is a very powerful mathematical process that evaluates the statistical significance of multiple parameters simultaneously. Experiments, in this context, means the execution of a computer simulation model. When dealing with complex or large scale systems, a large number of factors may have an impact on the performance of the system. Instead of changing the values one factor at time (OFAT) to determine how it will affect the system's performance, DOE allow us to vary all the factors simultaneously; thus, we save time

and money by gaining the maximum information out of a limited number of computer simulation runs.

The terminology of DOE methodology denotes the term "factor" for the input parameters and the term "response" for the output parameters of the simulation model. A level of a factor is the values that we assign to it during the experiment. Factors can be controllable (such as the aircraft's altitude) or uncontrollable (such as wind the speed) and qualitative or quantitative (Law 2015). This section uses DOE methodology to initially explore the effects and interactions among five input parameters (or factors) that are supposed to have an impact to the performance (or response) of the UCAV-based HEL weapon.

The DOE methodology usually consists of two steps. The first one, often the 2^k full factorial design method, gives an initial estimate for the significance of each parameter and allows for discarding the insignificant ones. It works as a screening phase which facilitates other design methods. This method calls for two levels for each parameter. The lowest and highest values of each parameter we are interested in will determine their range. A consultation of a subject matter expert is often recommended so that the range chosen is reasonable.

Assigning two values for each of the k design parameters produces 2^k possible combinations, called the *design points*. The totality of all these design points constitutes the *design matrix,* which is the actual set of input parameters for the simulation model; each design point in the matrix requires a separate simulation run with a distinct response value.

Response Surface Method

The number of controllable factors used in this part of the study (five) is low enough to allow skipping the screening phase (2^k factorial design) and to proceed directly to Response Surface Method (RSM), which includes additional design points midway between the two extreme values to give a better understanding of how the response behaves. For example, it can show quadratic dependencies between the factors and responses. Using this method, we can create a metamodel, usually a second order regression equation that may be used to estimate other sets of factor values. Additionally, we can use this metamodel to maximize or minimize the response.

Workflow Overview

To give a better idea to the reader of the DOE workflow, Figure 4 shows the steps followed. The first step is the selection of the input parameters we want to examine and their corresponding lower and higher values. Entering these values into Minitab, we then create the design matrix. Each design point in the matrix is run in WaveTrain (executed by Dr. Pogue) multiple times using different random seeds for the turbulence phase screen generation; thus, for each design point we get a distribution of peak irradiances and PIB (responses) to account for the random fluctuations due to turbulence. We then use this set of response values for the analysis, again using Minitab, to determine the statistical significance of each factor and produce a variety of plots.

The simulated engagement scenario assumes a UCAV patrolling in a predetermined area, receiving a call for fire upon a ground stationary target with an approximate height of 10m located at 180° azimuth, and examining the performance of the HEL weapon for different laser design configurations and UCAV tactics. The slant range between the platform and the target is held constant at 5000m as we vary the altitude of the UCAV. Various environmental models are utilized within WaveTrain to estimate the extinction coefficients (MODTRAN), the wind speed (wind direction constant from 90°) (Bufton), the atmospheric turbulence (Hufnagel-Valley 5/7) and the temperature (US Standard 76), all as functions of the altitude. The operating wavelength

of the HEL weapon is 1064nm. Table 2 presents the input parameters used as well as their corresponding levels.

FIGURE 4. DOE Workflow. The statistical package Minitab was used for the experimental simulation design generation and the output analysis, whereas the full diffraction code, WaveTrain, was used for the laser beam propagation simulation. All WaveTrain simulations were executed by Dr. Pogue.

TABLE 2. Input parameters with corresponding levels.

Factor	Levels
Output Power (kW)	50 – 150
Beam Director Diameter (m)	0,2 – 0,5
UCAV Altitude (m)	300 – 4000
UCAV Speed (m/s)	80 – 130
UCAV Direction (degrees)	0 – 90

The output power range (50kW – 150kW) is used because those value are more feasible, based on the current technology, to be mounted in a platform of the size of a UCAV. The beam director size range is a typical range of values used for HEL weapons. The flight altitude level was selected from 300 m to 4000 m as a nominal altitude range for a UCAV-HEL. Flying at higher altitudes would further decrease the horizontal effective range of the weapon. The speed range, from 80 m/s to 130 m/s, again is a representative of a UCAV such as the General Atomics MQ-9 Reaper. The direction levels, from northern to eastern courses, were selected to examine the wind effects on the HEL performance. Since the wind direction is held constant (90°), these two levels provide insights for its effects while perpendicular or parallel, respectively.

RESULTS AND ANALYSIS

DOE methodology requires that three assumptions are fulfilled in order to say that the resultant model is valid. Therefore, before proceeding with the analysis of the simulation results, we have to make sure that they are fulfilled. These assumptions have to do with the residuals (the difference between the WaveTrain simulation results and the results from the model's analytical fit) and are the following:

1) The errors are normally distributed with mean zero.

2) The error variance does not change for different levels of a factor or according to the values of the predicted response.

3) Each error is independent of all others. The best way to obtain independent errors is to randomize the run order of the experimental trials. Minitab does this by default.

The best way to determine the fulfillment of these assumptions is graphically using residual plots. Violation of these assumptions may lead to misleading results, though a transformation of the response can often be used to fix the problem (Oehlert 2010).

Statistical Analysis (Peak Irradiance)

We begin our analysis by asserting the model validity with regard to the peak irradiance. The same process was followed, but not presented in this paper, for the PIB. Figures 5 and 6 show the normal probability and "versus fits" plots for the peak irradiance, respectively.
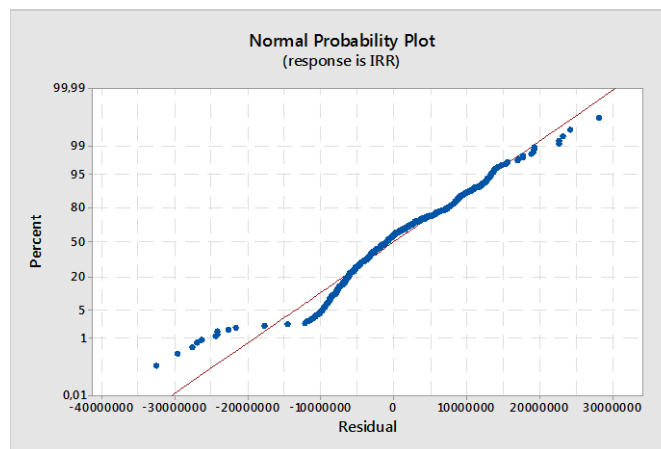
FIGURE 5. Normal Probability plot for irradiance. The residuals exhibit a non-linear pattern, something that indicates a non-normal distribution that violates the first DOE assumption.
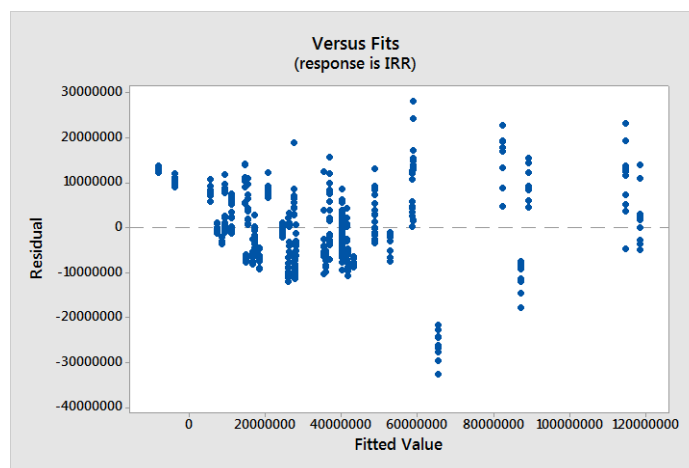
FIGURE 6. Versus fits plot for irradiance. The variance of the residuals is non-constant over the range of the fitted values and violates the second DOE assumption.

The blue dots represent the design points. Normal distributed residuals would give an approximate straight line (red line). This graph indicates that the first assumption of normality is violated. We can clearly see that the results follow a pattern other than the straight line.

The versus fits plot shows the difference that each observed value (obtained by the simulation) has from the value that the fitted mathematical model would give for the same set of factor values. This graph shows that the error variance increases for higher fitted values, indicating that the constant variance assumption is also violated.

Since this failed to fulfill both model assumptions, we cannot use this model for our analysis. Rather, we will use a response transformation to fit a more accurate model (Oehlert 2010). In this case, each design point's response is transformed by taking its natural logarithm. Then, as shown in Figure 7, the residuals for the design points now follow the ideal case more closely, therefore satisfying the first assumption. Note that the horizontal axis scale has now changed, since we are using the natural log of the peak irradiance value.
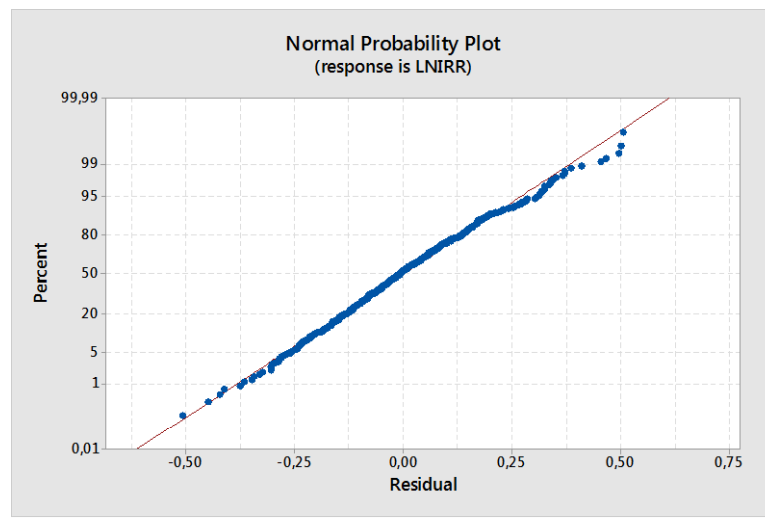
FIGURE 7. Normal Probability plot for the transformed response. A natural logarithm transformation on irradiance appears to alienate the issue of the non-normal distributed residuals.

The "versus fits" plot also is improved and shows that residuals are randomly distributed all along the response's value range, as shown in Figure 8. Again, both axis scales have changed to their natural logarithm of the response.

We then generate the main effects plot of each factor, as shown in Figure 9, to examine the effect of each factor on the mean transformed response to compare their relative importance. The vertical axis indicates the natural logarithm of peak irradiance and the horizontal axis the levels used in the design. The steeper the line, the greater the factor's effect on the response. We can see that the altitude's effect is the greatest; however, reaching the 4000m upper level shows that the slope decreases, indicating that we won't gain much by operating at higher altitudes. The same phenomenon occurs with the output power values, where at the level of 150kW the slope is much less than at lower powers. The same is not the case for the beam director size, where we see that it has an almost linear relation with the irradiance. Note also that the response lines for speed and direction have a very small slope indicating a small influence on the irradiance.
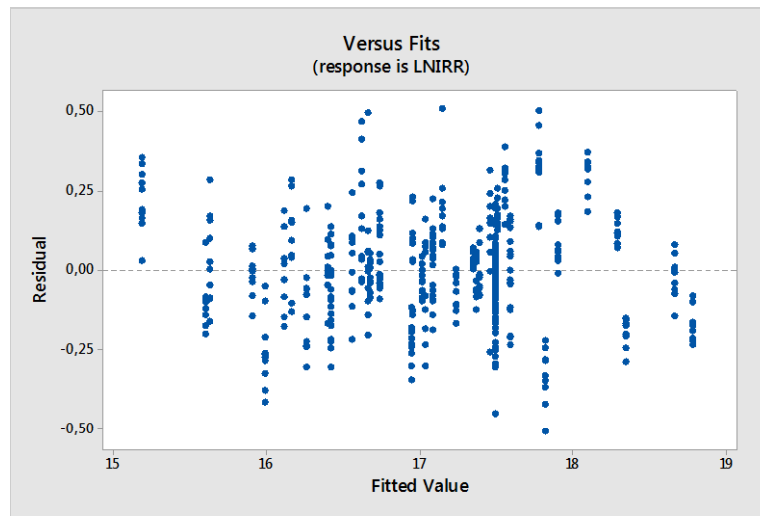
FIGURE 8. Versus fits plot for the transformed response. A natural logarithm transformation on irradiance appears to remove the issue of the non-constant variance of residuals.
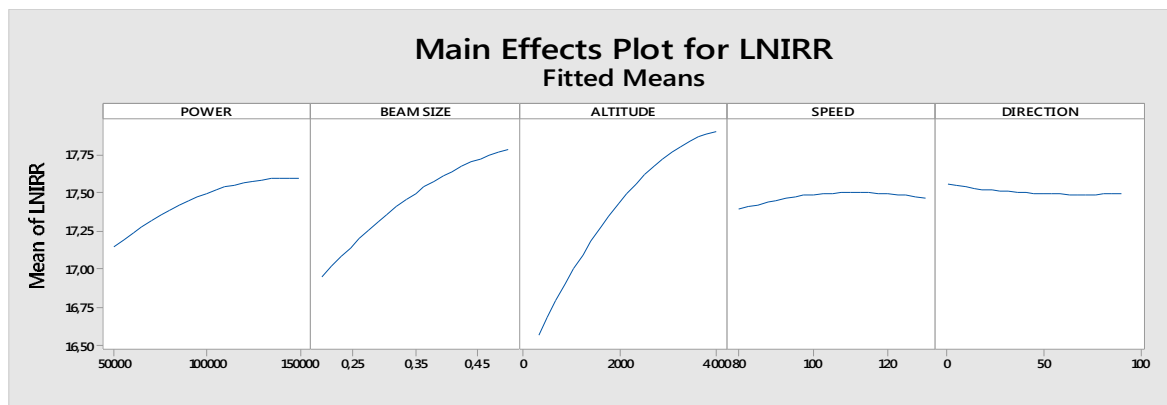
FIGURE 9. Main Effects plot for LN Irradiance for laser output power (in watts), beam director diameter (in meters), platform altitude (in meters), platform speed (in m/s), and platform direction (in degrees azimuth). Altitude has the most significant effect to the peak irradiance, followed by beam director size and power. Speed and direction seem to have only minor effects on the response.

As stated before, the simulation tool used for these first 600 runs is slow and required almost 24 hours to complete. Therefore, the advantage of fitting a statistical model to those randomized results is obvious, especially because they can easily be manipulated and reused for further analysis. To further validate the accuracy of our statistical model, after having generated the contour plot shown in Figure 10 (left plot) from the statistical model, we then ran the same parameters through WaveTrain. As shown in Figure 10, a graphical comparison of the statistical model and the WaveTrain results indicate that the main pattern follows the same trends. This occurs for both peak irradiance and PIB, as shown in Figure 11.
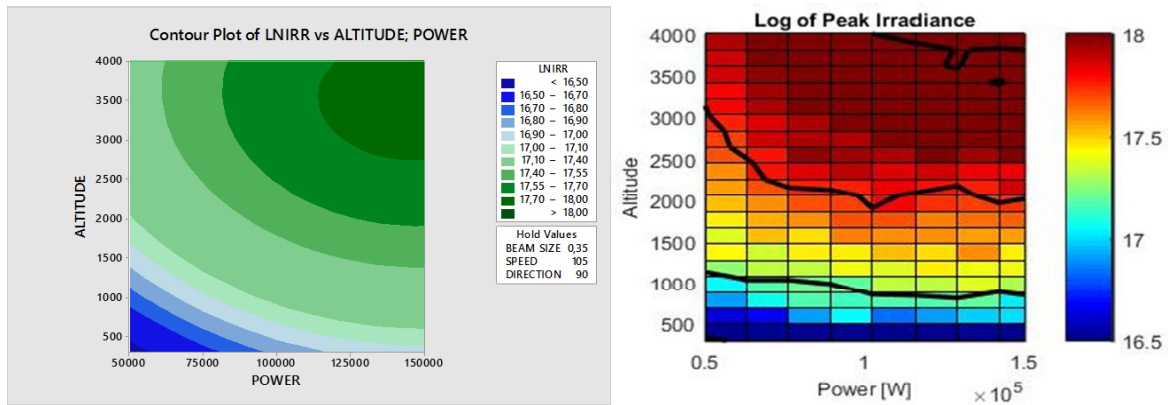
FIGURE 10. Model Comparison between Minitab and WaveTrain for the natural log of the peak irradiance on target. The main pattern of the contour lines, which is of most interest for this study, seem to follow the same trends as the ones from Minitab. Starting from a 50 kW power, it has a negative slope that, by the level of around 150 kW, has stabilized. Both plots also exhibit predict a similar spread in peak irradiances.
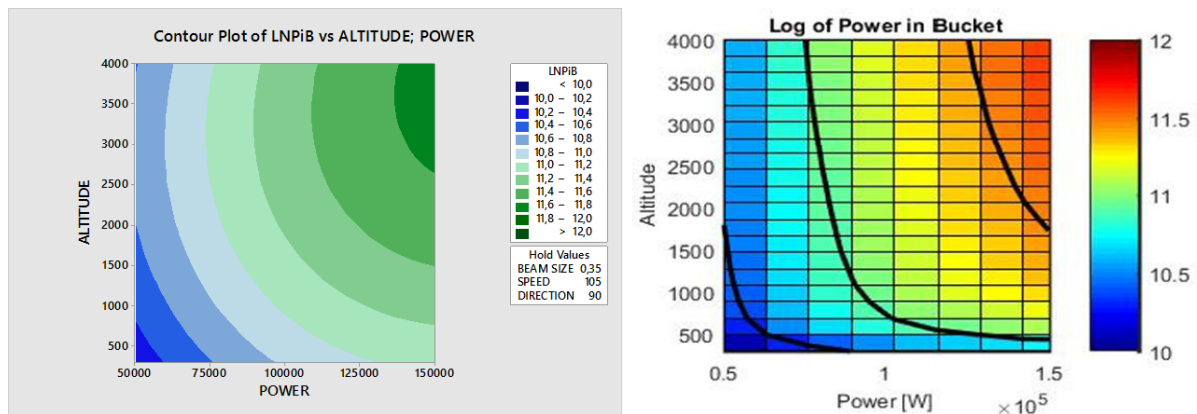
FIGURE 11. Model Comparison between Minitab and WaveTrain for power-in-bucket. Both models show similar trends for the relation between altitude and output power for PIB. Namely, at higher platform altitudes, there is a clear advantage to larger output power; at lower altitudes, atmospheric effects delay the benefits of increased output power. The contour area of interest (left plot) lies within the contour lines of 11.2 and 11.4 which correspond to a PIB between 74kW and 90kW. That allows us to identify possible alternatives that could achieve the same PIB.

We can now further analyze the statistical results in Minitab, and in particular the contour plot for altitude versus power. Figure 11 (left plot) shows the PIB achieved for all combinations of UCAV altitude and HEL power that were considered. As calculated in Figure 3, the required PIB to melt the predetermined area in the target is approximately 85 kW. The area that satisfies this requirement lies within the 11.2 and 11.4 contour lines which corresponds to 74kW and 90kW PIB, respectively. Therefore, this contour region sets the approximate threshold for a successful engagement (as defined earlier). Figure 11 (left plot) indicates that different HEL designs could achieve similar PIBs by operating from different altitudes. For example, an HEL of 150kW on a UCAV flying at 1000m and an HEL of 100kW on a UCAV flying at 3000m both deliver about the same PIB, even though the target remains 5000m from the UCAV for both cases. This fact illustrates the advantage offered by operating in higher altitudes, which places the platform above much of the harmful atmospheric effects at lower altitudes.

Weight Estimation

Having identified two alternatives that could achieve the same level of performance, measured by the PIB delivered to the target, we then can estimate the weight of each one—an important consideration for UCAV operation and endurance. In order to calculate the weight of an HEL, we have to separately estimate the weight of the laser module itself, W_L, the weight of the energy storage subsystem, W_{ES}, the weight of the thermal management subsystem, W_T, and the weight of beam director subsystem, W_{BD} (Motes and Berdine 2009).

Precise values of these weights are not know and would depend on the exact design of the HEL; however, publically available information does provide some guidance on the weights of these subsystems. In particular, we use the power to weight ratio (5kg/kW) of the HELLADS laser system developed by General Atomics (General Atomics 2016), the specifications of a typical lithium-ion battery with energy density 0.36MJ/kg (Panasonic 2016) with a storage capacity sufficient for a total of 60 seconds dwell time, the specifications of Thermal Energy Storage technology developed by RINI (RINI Technologies 2016), and the OTHELA beam director subsystem developed by MZA.

Table 3 summarizes the weight estimations for each main subsystem for both alternatives.

Table 3. Weight Estimations for HEL Subsystems.

	150 kW	100 kW
Energy Storage Subsystem Weight (kg)	108	72
Laser Module Weight (kg)	750	500
Beam Control Subsystem Weight (kg)	225	225
TES Weight (kg)	590	392
Total HEL Weight (kg)	**1670**	**1190**
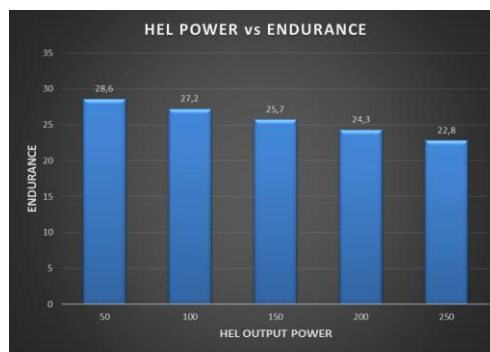
Figure 12. UCAV Endurance versus HEL Output Power. We assumed a linear relationship between UCAV endurance and payload weight.

The next step of the analysis is to determine how the endurance of the UCAV will be affected by the weight of each alternative. By consulting a field subject matter expert, the CEO of Vstar Systems Inc., a simple mathematical expression relating the endurance of the UCAV with the payload weight is constructed. Assuming the total payload weight comes from the weight of the HEL, the UCAV endurance for the various output power levels is calculated, as shown in Figure 12.

In particular, we can see that the higher power (150kW) alternative allows for an endurance of approximately 25.5 hours, whereas the lower power (100kW) alternative allows for an endurance of 27 hours.

Jitter and Beam Quality Study

The WaveTrain simulation runs to generate the analytic model did not incorporate beam quality and platform jitter. Therefore, we had to execute additional simulation runs using ANCHOR, which is capable of examining beam quality and platform jitter effects on the HEL performance. While keeping the previously used design parameters constant, we vary the beam quality and jitter value, from the ideal situation with no jitter and perfect beam to a more realistic one. Table 4 summarizes the input parameters used in ANCHOR simulation runs.

Table 4. Input Parameters Used in ANCHOR

Wavelength λ	1.064 µm
Target Height H_T	Varies
Beam Director Size D	0.35 m
Beam Shape at Source	Uniform
Platform Direction	North
Wind Direction	90°
Target Speed V_{target}	0 m/s
Platform Speed V_{UCAV}	105 m/s
Power-in-the-Bucket Size r_b	0.05 m
Fractional Target Absorption	0.2
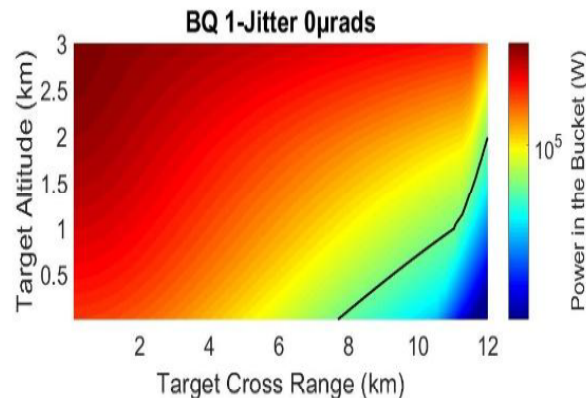
Figure 13. Contour Plot for Altitude versus Range. This plot refers to the ideal situation where beam quality is perfect and we have zero platform jitter. The effective range of the HEL is indicated by the contour line, which indicates the PIB threshold estimated earlier.

Figure 13, shows the output from a simulation run in ANCHOR for a UCAV flying at 3000m altitude and armed with a 150kW HEL. The response in this particular plot is the PIB and the contour line indicates the previously estimated threshold to melt the target. The horizontal axis represents the cross range to the target, whereas the vertical axis represents target's height above ground. The effective range achieved in this case is the maximum possible and could only occur under an ideal situation (where the beam quality metric M^2=1 and platform jitter is zero).
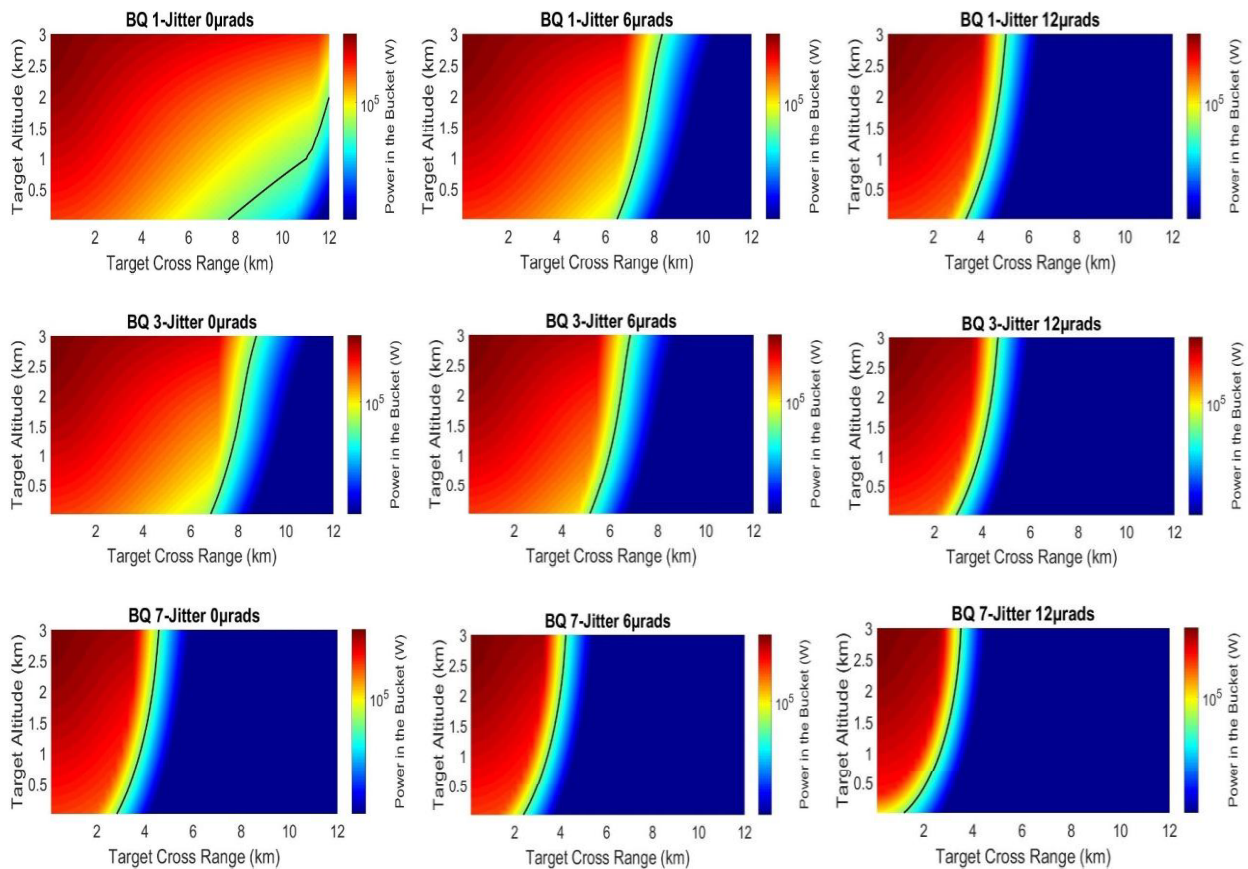
Figure 14. Platform Jitter and Beam Quality Effects. Starting from the upper left plot, which shows the ideal situation (M^2=1 and jitter=0), we see that the HEL's effective range is almost 8km. The lower right plot (M^2=7 and jitter=12μrad) shows the significant decrease of the effective range down to almost 1km.

To better visualize the effects that beam quality and platform jitter have to the PIB, Figure 14 shows a collection of equivalent plots, where M^2 (a beam quality metric where M^2>1 imperfect beam quality) and platform jitter are changing. Moving to the right, we see the effects of the platform jitter for 6 μrad and 12 μrad root-mean-square values, respectively. Moving downwards, we see the effect of a beam quality of M^2=3 and M^2=7, respectively. Looking at the worst case scenario, the lower right plot, we can see that with a beam quality M^2=7 and an average platform jitter of 12 μrad, the effective range of the HEL (indicated by the contour line) goes from almost 8km at ground level for the ideal situation to slightly more than 1km, indicating the strong effects of both parameters.

CONCLUSIONS

This paper presents a case study utilizing DOE in the simulation analysis. The advantages of this process are evident in terms of time and cost. A single simulation model and a nominal number of runs were sufficient to give us a clear understanding of the effects that the included factors have to the performance measure of our system, including their interactions. We managed to fit a mathematical model and gain confidence that it would give us valid predictions by direct comparisons to output from WaveTrain. By incorporating factors related to the UCAV tactics and the HEL design, we were able to establish that the operating altitude has the

strongest influence on performance of the weapon and that higher operating altitudes, if possible, could compensate for lower output power and smaller beam director size. This is a significant result if we consider the SWaP constraints for a UCAV. The weight estimation of a 100kW and a 150kW HEL weapon shows that both could be mounted in a UCAV with payload capabilities similar to those of Predator B. The lower weight of the first one results in an endurance increase of about one and a half hours, whereas the higher power of the latter would help compensate for the negative effects of the worse beam quality and higher platform jitter.

REFERENCES

1. Defense One. "Drones Armed with High Energy Lasers May Arrive in 2017." September 2015. http://www.defenseone.com/technology/2015/09/drones-armed-high-energy-lasers-may-arrive-2017/121583/.
2. O'Rourke, Ronald. 2015. *Navy Shipboard Lasers for Surface, Air, and Missile Defense: Background and Issues for Congress*. CRS Report No RL41526. Washington, DC: Congressional Research Service. https://fas.org/sgp/crs/weapons/R41526.pdf.
3. Valiani, Joshua 2016. "Power and Energy Storage Requirements for Ship Integration of Solid-State Lasers on Naval Platforms". Thesis, Naval Postgraduate School, Monterey.
4. Law, Averill M. 2015. *Simulation Modeling and Analysis*. 5th ed. New York: McGraw- Hill Education.
5. Oehlert, Gary W. *A first course in design and analysis of experiments.* 1st ed. 2010.
6. Perram, G. P., S. J. Cusumano, R. L. Hengehold, and S. T. Fiorino. 2009. Introduction to Laser Weapon Systems, 1st ed. Albuquerque, NM: Directed Energy Professional Society.
7. Sofieva, V. F., F. Dalaudier, J. Vernin. 2013. *Using Stellar Scintillation for Studies of Turbulence in the Earth's Atmosphere.* Philosophical Transactions of the Royal Society A. 371(1982).
8. Rini Technologies. 2016. "Thermal Energy Storage (TES) Technology." http://rinitech.com/wp-content/uploads/2016/01/ThermEnergyStorage.pdf
9. Coy S. 2013. WaveTrain: A User-friendly Wave Optics Propagation Code [Online]. Available: https://www.mza.com/publications/wtspiepaper.htm.
10. Motes, Andrew R., and Richard W. Berdine. 2009. *Introduction to High-Power Fiber Lasers*. 1st ed. Albuquerque, NM: Directed Energy Professional Society.
11. General Atomics Aeronautical. 2016. "HELLADS". http://www.ga-asi.com/hellads.
12. Panasonic 2016. "Rechargeable Batteries: Lithium Ion Batteries (Li-lon)". Access date November 19. https://na.industrial.panasonic.com/sites/default/pidsa/files/downloads/files/panasonic_overview_information_on_li-ion_batteries.pdf
13. General Atomics Aeronautical. 2016. "HELLADS". http://www.ga-asi.com/hellads.